Australian Journal of Earth Sciences (2005) **52**, (529–544)

Geology of five small Australian impact craters

E. M. SHOEMAKER,[1] F. A. MACDONALD[2]* AND C. S. SHOEMAKER[3]

[1]*Died 18 July 1997.*
[2]*Department of Earth and Planetary Sciences, Harvard University, 20 Oxford St., Cambridge, MA 02138, USA.*
[3]*US Geological Survey, Shoemaker Astrogeology Center, 2255 North Gemini Drive, Flagstaff, AZ 86001, USA.*

Here we present detailed geological maps and cross-sections of Liverpool, Wolfe Creek, Boxhole, Veevers and Dalgaranga craters. Liverpool crater and Wolfe Creek Meteorite Crater are classic bowl-shaped, Barringer-type craters. Liverpool was likely formed during the Neoproterozoic and was filled and covered with sediments soon thereafter. In the Cenozoic, this cover was exhumed exposing the crater's brecciated wall rocks. Wolfe Creek Meteorite Crater displays many striking features, including well-bedded ejecta units, crater-floor faults and sinkholes, a ringed aeromagnetic anomaly, rim-skirting dunes, and numerous iron-rich shale balls. Boxhole Meteorite Crater, Veevers Meteorite Crater and Dalgaranga crater are smaller, Odessa-type craters without fully developed, steep, overturned rims. Boxhole and Dalgaranga craters are developed in highly foliated Precambrian basement rocks with a veneer of Holocene colluvium. The pre-existing structure at these two sites complicates structural analyses of the craters, and may have influenced target deformation during impact. Veevers Meteorite Crater is formed in Cenozoic laterites, and is one of the best-preserved impact craters on Earth. The craters discussed herein were formed in different target materials, ranging from crystalline rocks to loosely consolidated sediments, containing evidence that the impactors struck at an array of angles and velocities. This facilitates a comparative study of the influence of these factors on the structural and topographic form of small impact craters.

KEY WORDS: Boxhole Meteorite Crater, Dalgaranga, Henbury Meteorite Craters, Liverpool, meteorite impact craters, oblique impact, Veevers Meteorite Crater, Wolfe Creek Meteorite Crater.

INTRODUCTION

Because of the arid nature of the Australian continent and its generally low topographic relief, small impact craters are extremely well preserved and readily accessible (Figure 1). Whereas meteorites from most of these craters have been studied in detail (Bevan 1996), few structural analyses of some of these craters have been carried out (Milton 1972). Here we present results from 12 field seasons in Australia studying 17 different impact structures and several 'false alarms'. We focus on structural and mechanical studies of Liverpool crater, Wolfe Creek Meteorite Crater, Boxhole Meteorite Crater, Veevers Meteorite Crater, and Dalgaranga crater.

Shoemaker and Eggleton (1961) identified two principal structural types of small impact craters. One type is exemplified by Meteor Crater (Barringer) in Arizona and the other type by the main Odessa crater in Texas (Figure 2); these two classes are often represented by the Teapot ESS and Jangle U nuclear-explosion craters at the Nevada Test Site (Shoemaker 1963), but here we use natural examples to classify natural craters. Beds exposed in the walls of Barringer crater, in general, dip gently outward low in the crater, and more steeply outward at higher levels, close to the contact with the ejecta. Locally, beds are overturned and uppermost beds are folded outward as a rim flap so as to reverse their stratigraphic succession. In places, the overturned flap is broken by nearly vertical tear faults, and grades outward into ejecta. Rock fragments in the entire ejecta blanket are stacked roughly in an inverted stratigraphic sequence. Other distinctive characteristics of a Barringer-type crater are steep walls ($\sim 45^{\circ}$) and a relatively thick breccia lens. These features imply much greater modification of the transient crater in the late stage of gravity modification than for smaller, Odessa-type craters. Beds exposed in the wall of Odessa crater are buckled in an anticline, and locally are displaced along inward-dipping faults (Evans & Mear 2000). Commonly, the top of the anticline is truncated and the crest of the rim is composed of ejecta (Figure 2). Liverpool and Wolfe Creek are Barringer-type craters, while Boxhole, Veevers, and Dalgaranga are Odessa-type craters.

Meteorites have been found at Wolfe Creek, Boxhole, Veevers, and Dalgaranga craters, and thus all are considered proven meteorite impact craters (Bevan 1996). Meteorite fragments have not been reported at Liverpool. Hence, despite extensive brecciation and a structural form characteristic of an impact crater, the Liverpool crater is conventionally referred to as a

*Corresponding author: fmacdon@fas.harvard.edu

ISSN 0812-0099 print/ISSN 1440-0952 online © Geological Society of Australia
DOI: 10.1080/08120090500180921

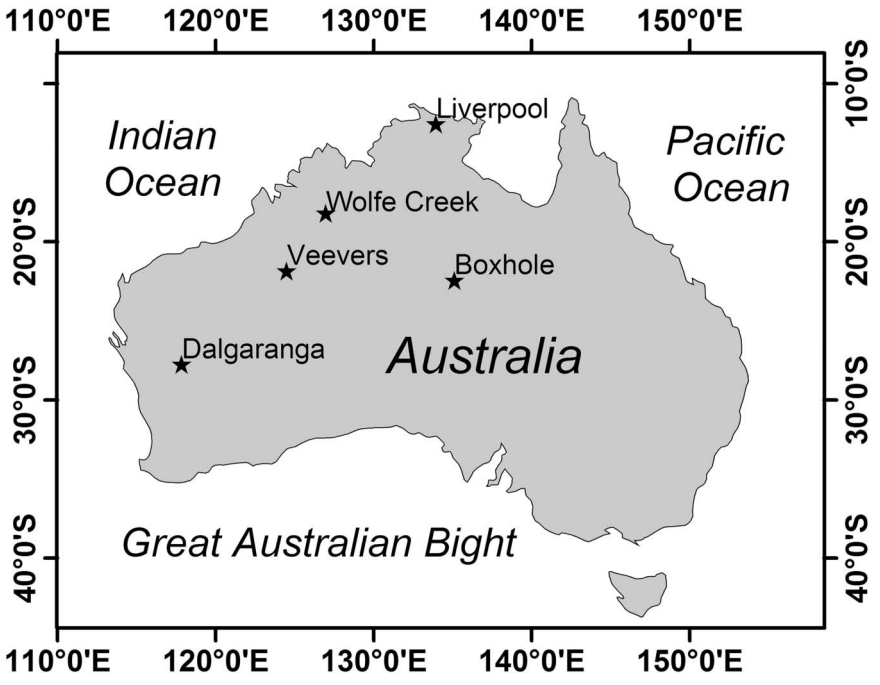

Figure 1 Locations of craters discussed in this study. With the exception of Liverpool crater, these small craters are all located in the arid outback of Australia.

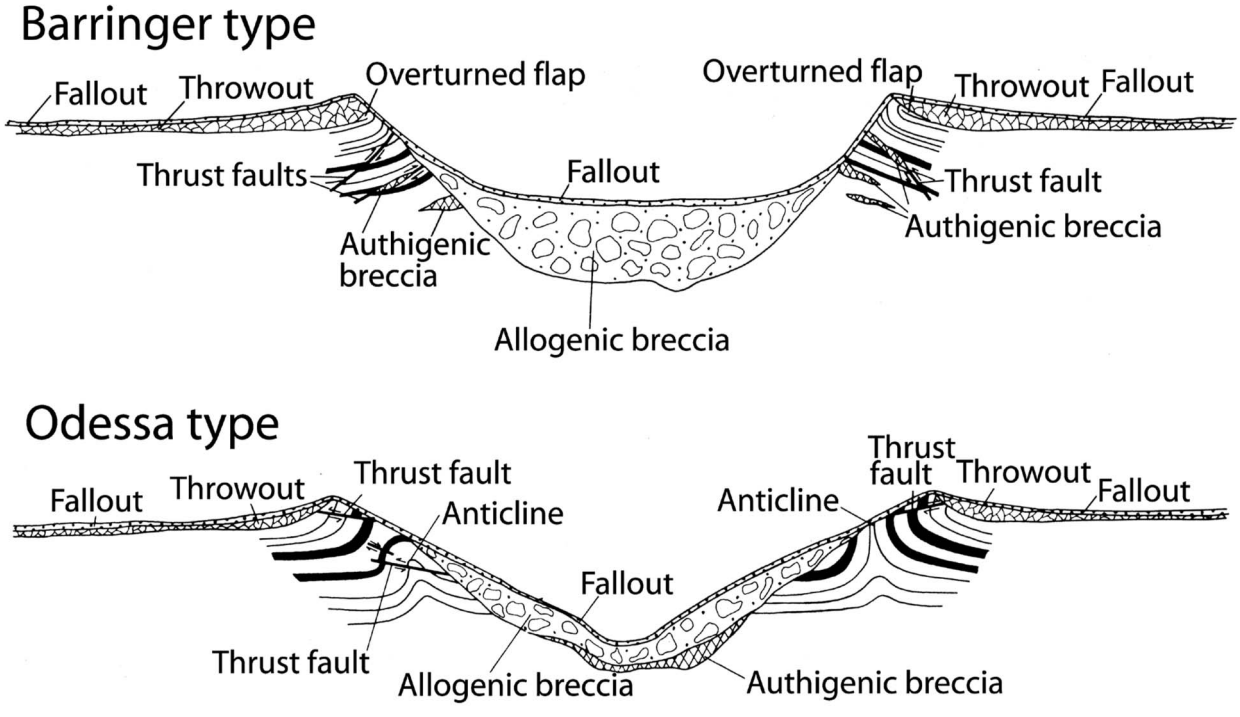

Figure 2 Schematic cross-sections illustrating the structure of the Barringer and Odessa types of craters (modified from Shoemaker & Eggleton 1961). Beds exposed in the walls of Barringer crater dip gently outward low in the crater and more steeply outward at higher levels, close to the contact with the ejecta. Locally, beds are overturned and the uppermost beds are folded outward as a rim flap so as to reverse their stratigraphic succession. Beds exposed in the wall of Odessa crater are buckled in an anticline, and locally are displaced along inward-dipping faults. The top of the anticline is truncated and the crest of the rim is composed of ejecta.

probable impact structure. We have ordered our discussion of these craters from largest to smallest, which also corresponds closely to a sequence from oldest to youngest. We give more exhaustive discussions to craters that have largely escaped previous scrutiny. For the benefit of modelling and experimental studies we have tried to include measurements of those variables important to the scaling of impact craters (Table 1).

Table 1 Location, age, and important scaling variables of craters discussed herein.

Crater features	Liverpool crater	Wolfe Creek Meteorite Crater	Boxhole Meteorite Crater	Veevers Meteorite Crater	Dalgaranga crater
Location	~50 km E of Jabiru, Arnhem Land, NT	~100 km S of Halls Creek, Kimberley, WA	~170 km NE of Alice Springs, NT	Canning Basin, Great Sandy Desert, WA	Yilgarn, Yalgoo Shire, WA
Latitude	12°23′30″S,	19°10′20″S,	22°36′45″S,	22°58′06″S,	27°40′00″S,
Longitude	134°02′45″E	127°47′40″E	135°11′47″E	125°22′07″E	117°17′30″E
Age	Neoproterozoic?	*ca* 300 ka[a]	*ca* 30 ka[a]	*ca* 4 ka?[b]	< 3 ka?[b]
Rim crest diameter	2000 m	825–935 m (av. 880 m)	170–190 m	72.5 m	23.5 m
Apparent diameter (from ground level)	1600 m	800 m	170 m	56.25 m	19 m
Original depth	230 m	150 m	30 m	15 m	5 m
Depth today	Filled	50 m	16 m	3 m	2 m
Rim height today	NA	35 m	5 m	3 m	1.5 m
Target material	Flat-lying Proterozoic sandstones	Devonian sandstones with laterite cover	~Vertical gneisses with colluvium cover	Flat-lying laterite	Archaean granites with colluvium cover
Meteoritic material discovered at site	None found	Iron, group IIIAB, and shale balls	Iron, group IIIAB	Iron, group IIAB	Stony-iron, mesosiderite
Maximum ejecta radius & direction	NA	~3000 m towards the SE	> 300 m towards the S	< 100 m towards the NE	< 60 m towards the N
Impact incidence (from horizontal)	45–30° from SW	45–30° from NE	< 30° from N?	60–45° from SW	~15° from SSE
Crater type	Barringer	Barringer	Odessa	Odessa	Odessa

[a] Shoemaker *et al.* 1990; [b] Shoemaker & Shoemaker 1988.
Original depth was estimated by projecting the original rim height and position of the crater floor from the attitudes of bedding planes and contact surfaces exposed in the crater walls. The ages of Veevers and Dalgaranga are accompanied with question marks because they are estimated from relative erosion of ejecta blankets (Shoemaker & Shoemaker 1988). The angle of incidence was estimated by comparing asymmetries in the craters and their ejecta with experimental results (Gault & Wedekind 1978). The estimated angle of incidence at Boxhole is accompanied with a question mark because the interpretation of asymmetries due to impact angle is complicated by the pre-existing structure and slope of the target rocks.

LIVERPOOL CRATER

Liverpool crater is a ~1.6 km-diameter, partially exhumed impact crater (Figure 3a), located in the Arnhem Land Aboriginal Reserve of the Northern Territory (12°23′30″S, 134°02′45″E: Figure 1), ~2 km northwest of the Liverpool River. Rix (1965) first mapped the regional geology of the Milingimbi 1:250 000-scale map sheet and recognised the site as a possible impact crater. The crater was briefly visited by Guppy *et al.* (1971), who gave a preliminary geological description and described planar features in quartz grains from breccias exposed in the crater walls. Shoemaker and Shoemaker (1997) completed a more comprehensive geological mapping of the Liverpool crater (Figure 4).

Bedrock exposed in the vicinity of the Liverpool crater includes the Palaeoproterozoic Gumarrirnbang Sandstone (formerly the Kombolgie Formation) and the Neoproterozoic Buckingham Bay Sandstone (Carson *et al.* 1999). The age of Gumarrirnbang Sandstone is constrained between the 1870–1850 Ma Barramundi Orogeny and the intruding 1688 ± 13 Ma Oenpelli Dolerite (Carson *et al.* 1999). The Gumarrirnbang Sandstone is a medium-bedded, generally medium-grained, quartzose sandstone with centimetre-scale cross-beds. Well-developed current ripples are common. Some beds are sparsely conglomeratic and contain well-rounded, white, vein-quartz pebbles up to 5 cm across. These exposures are along the eastern margin of an extensive, extremely rugged, dissected plateau underlain by nearly flat-lying Gumarrirnbang Sandstone, which extends some 50 km to the west, almost to Jabiru, and to within 200 m southwest of the Liverpool structure. Two prominent, regional joint sets are developed in the sandstone, trending 20°W and 50°W.

The Gumarrirnbang Sandstone is abruptly upturned and brecciated at the margin of the impact structure, forming an authigenic breccia (Figure 4). This zone of deformation has a sharp outer boundary against very gently deformed Gumarrirnbang Sandstone. In places, there are large, structurally coherent zones within the breccia, in which the sandstone beds are nearly vertical or overturned. Near the outer boundary of impact deformation, overturned sandstone blocks dip toward the centre of the crater at angles of 45–50°. Generally, the authigenic breccia consists of angular clasts up to ~10 cm across, with occasional metre-scale blocks set in a matrix of crushed sandstone, and criss-crossed with silica-cemented fractures. Large coherent zones near the crater wall are commonly only lightly fractured, but, where exposed nearest the crater centre in the southwest quadrant of the structure, the rocks are pervasively crushed and shattered. The most intensely shocked material exposed is found in the matrix of these innermost exposures.

Allogenic breccia makes up most of the exposed breccia ring at Liverpool crater (Figure 3a). The

Figure 3 (a) Oblique aerial photograph of the Liverpool crater taken from the north. The white ring of resistant rock is allogenic breccia, which is cut by several small streams. The outer diameter of the ring of allogenic breccia measures ~1.6 km. (b) Oblique aerial photograph of Boxhole Meteorite Crater taken from the southwest. The white material around the rim is ejecta, whereas the light-orange material with very little vegetation is reworked ejecta and ejecta covered with a veneer of alluvium. The east–west-trending vegetated ridge on the northern side of the crater is composed of metamorphosed quartzite mantled with colluvium.

allogenic breccia rests in knife-sharp contact with authigenic breccia or Gumarrirnbang Sandstone. The grooves plunge roughly toward the centre of the structure, indicating outward radial transport of the basal breccia. In most places, the basal contact of the allogenic breccia dips inward at angles of 40–50°, but in the broad exposure of breccia in the southwest quadrant of the structure it is a rolling surface with an ~5° average inward dip (Figure 4). Clasts in the allogenic breccia range from sand splinters to blocks several metres across. About half the bulk of the breccia consists of angular to subrounded clasts ~10–30 cm across. Unlike the authigenic breccia, hardly any clasts in the allogenic breccia are crushed or deformed. The allogenic clasts appear to have come from regions high on the crater walls that were exposed to relatively low shock stresses. The lithology and bedding characteristics in the individual clasts are similar to those seen in the undeformed Gumarrirnbang Sandstone southwest of Liverpool crater. A remarkable feature of the allogenic breccia is a crude stratification. In places, the breccia consists of multiple discrete units with well-defined contact surfaces. Abrupt changes in texture and clast size occur across some contacts. Evidently the breccia was emplaced as a sequence of discrete slumps or flows. Dips in the individual flow units are in the range of 20–25° around most of the structure, but on the southwest side, they follow the rolling contact with the underlying authigenic breccia.

A sequence of crater-fill units was mapped interior to the breccia ring consisting of a basal sedimentary breccia unit and an upper unit of sandstone. The sedimentary breccia rests in sharp contact above the allogenic breccia on the northwest, northeast and southeast sides of the crater and is crudely, but distinctly, bedded. Clast sizes generally are less than 20 cm, and the matrix is more fine-grained than in the allogenic breccia. Observed dips average about 15° toward the centre of the structure.

About 30 m of well-indurated, gritty sandstone constitutes the upper member of the preserved crater-fill sequence. A ring of the sandstone member is well exposed near the centre of the structure. The contact of the sandstone with the underlying sedimentary

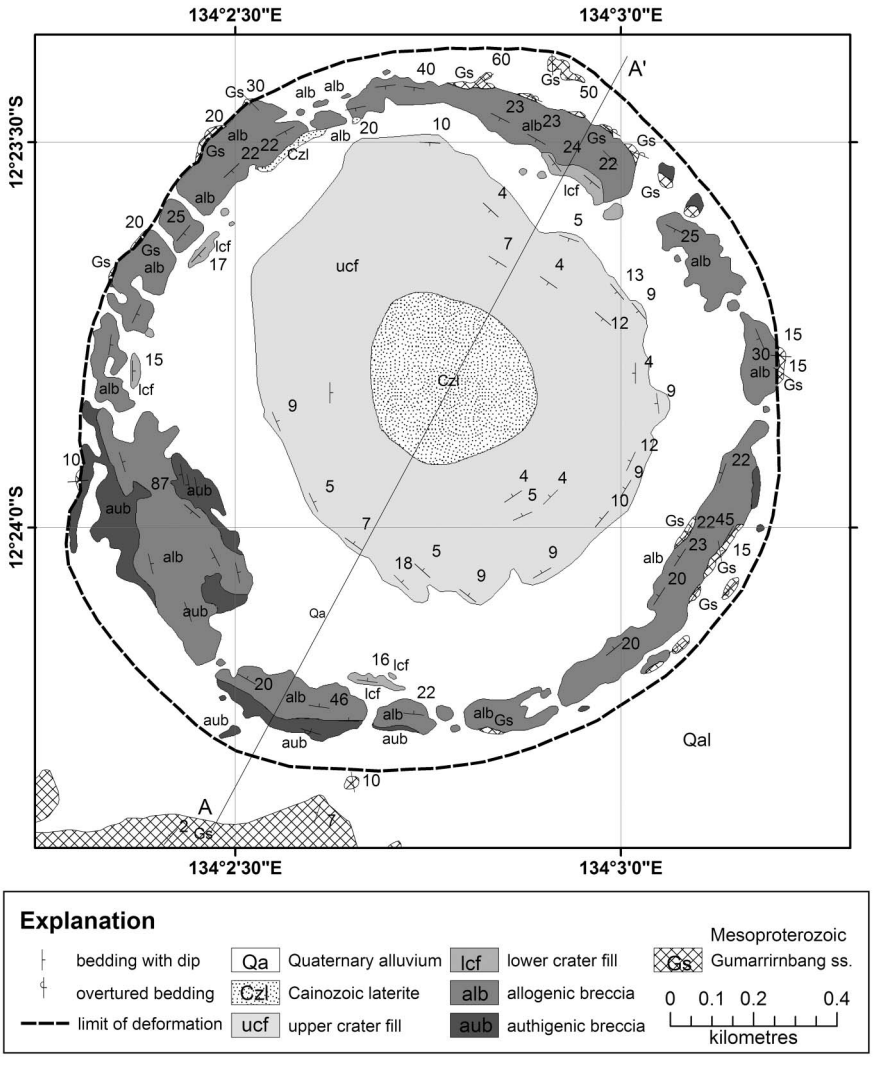

Figure 4 Geological map of the Liverpool crater, compiled by E. M. Shoemaker in 1996. Notice the slight elongation of the crater on the north-northeast–south-southwest axis and the offset of the central region towards the north-northwest. See Figure 5 for cross-section A–A'.

breccia member is concealed everywhere by alluvium. Beds in the upper member are locally conglomeratic and contain quartz pebbles up to 5 cm across that have been reworked from Gumarrirnbang Sandstone. Rarely, sandstone pebbles are present, which distinguishes the crater fill units from Gumarrirnbang Sandstone. Dips in the upper member of the crater fill range from 4° to 18° and become progressively shallower toward the centre of the structure. As sedimentary structures in the sandstone member indicate that the beds were laid down horizontally, existing dips are probably due to compaction.

The crater-fill units at Liverpool appear similar the basal units of the Neoproterozoic Buckingham Bay Sandstone in the Wessel Group (P. Haines pers. comm. 2004). The Buckingham Bay Sandstone is commonly cross-bedded, moderately well sorted, medium- to coarse-grained, and medium to thickly bedded; bedding thins progressively upsection (Carson *et al.* 1999). The basal unconformable contact between the Buckingham Bay Sandstone and older rocks is marked locally by a basal conglomerate or regolith breccia. This basal unit is several metres thick and contains poorly sorted angular clasts up to boulder size in a sandy matrix. The Buckingham Bay Sandstone outcrops ~2 km northeast of the Liverpool crater where it unconformably overlies the Gumarrirnbang Sandstone (Carson *et al.* 1999; P. Haines pers. comm. 2004). A Late Neoproterozoic age is assigned to the Wessel Group on the basis of the large acritarch *Chauria circularus* found directly above the Buckingham Bay Sandstone in the Raiwalla Shale (Carson *et al.* 1999).

The Liverpool impact structure is about 6% broader in the northeast–southwest direction than in the northwest–southeast direction (Figure 4). This difference, due chiefly to broad zones of authigenic breccia and strongly deformed Gumarrirnbang Sandstone on the southwest and northeast sides, probably reflects the direction of impact. Moreover, the centre of the depositional basin within the crater is offset about 100 m to the northeast from the centre of the structure, and strata are more overturned in the northeast than in the southwest crater walls (Figure 5). These relationships indicate that the direction of travel of the impactor was from the southwest. However, the ring of exposed allogenic breccia is nearly circular and does not reflect asymmetries found in the authigenic breccia, nor in the crater walls. The basal allogenic breccia contact has an

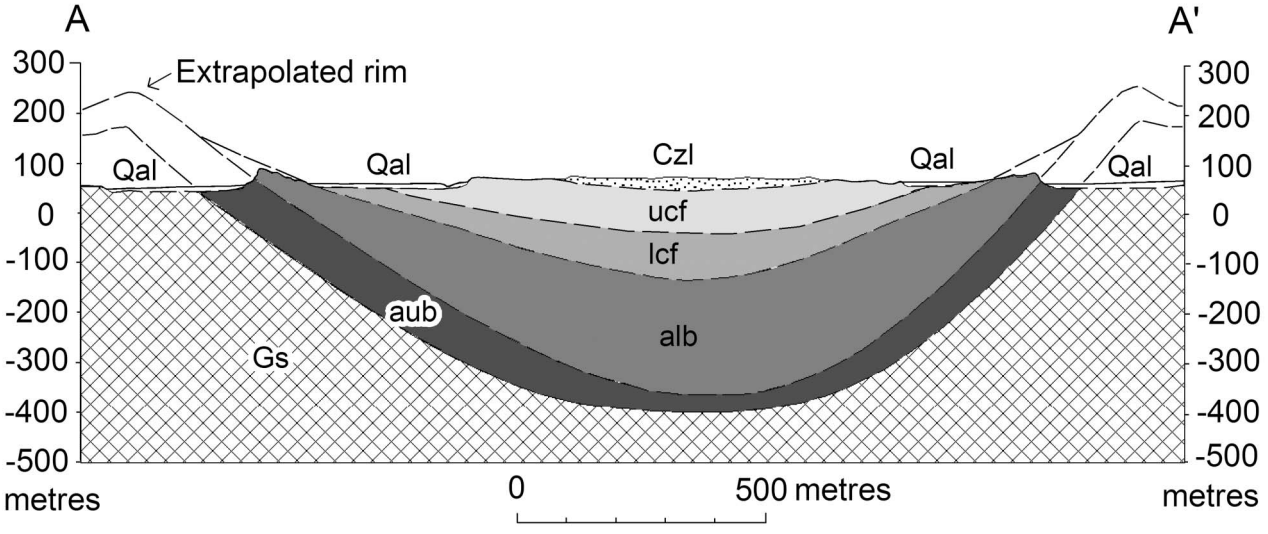

Figure 5 North-northeast–south-southwest geological cross-section of the Liverpool crater (see Figure 4 for location). The crater-fill units (lcf & ucf) are probably of Late Neoproterozoic age (Buckingham Bay Sandstone), yet much of the crater form and impact breccia are preserved under the fill, indicating a prompt burial after the impact and a recent exhumation. The rim height, and the position of contacts and thicknesses of units at depth were estimated by projecting from attitudes of bedding planes and contacts between units exposed in the crater walls.

average dip of 45°. Projecting this relationship outwards to the limit of strongly deformed bedrock implies that 100–200 m of crater rim have been lost to erosion and that the original crater was ~20% larger than the diameter of the preserved allogenic breccia ring. Although Guppy *et al.* (1971) suggested that the crater fill might be Cretaceous in age, the similarity between the crater-fill units and the basal Buckingham Bay Sandstone, both in terms of sedimentary structure and induration, suggests a Late Neoproterozoic age of the crater-fill. A Neoproterozoic age of the impact is also inferred, as the shallow level of erosion indicates that the Liverpool crater was buried soon after formation. Incised valleys and Cenozoic laterites within the crater indicate that it was exhumed during or prior to the Cenozoic (Carson *et al.* 1999).

WOLFE CREEK METEORITE CRATER

Wolfe Creek Meteorite Crater is situated at 19°10′20″S, 127°47′40″E on the eastern margin of the Great Sandy Desert, Western Australia (Figure 1), about 100 km south of Halls Creek. The crater was first described by Reeves and Chalmers (1949), and named after Wolfe Creek, which runs north–south, ~3 km west of the crater. Early reports used the spelling 'Wolf'. An impact age of 300 ka was obtained from cosmogenic radionuclide dating of meteorites found near the crater (Shoemaker *et al.* 1990). The crater rim stands 35 m above the surrounding plain and is slightly elliptical in plan view (Figures 6, 7). Wolfe Creek Meteorite Crater measures ~935 m on a north-northeast–south-southwest axis and ~825 m on a west-northwest–east-southeast axis, and has an average diameter of 880 m (Figure 7) (Hawke 2003). Gravity data suggest an original crater depth of ~150 m with no large meteoritic mass preserved in the floor (Fudali 1979; Hawke 2003). Sediments fill the crater to a current rim-to-floor depth of ~50 m.

A recent aeromagnetic survey over Wolfe Creek Meteorite Crater, undertaken by the Geological Survey of Western Australia, reveals a multi-ringed feature (Figure 6). Line spacing of the aeromagnetic survey was 50 m over a 4 x 4 km area, with a nominal terrain clearance of 40 m, although aircraft altitude varied between 30 and 60 m, especially within the crater area (Hawke 2003). Two concentric circular anomalies correlate respectively with the crater rim and the base of the inner crater walls (at an ~700 m diameter: Hawke 2003).

Pre-crater structure at Wolfe Creek dips gently to the south and the lowest beds are exposed in the north crater wall. Devonian sandstones exposed in the crater walls (Myers & Hocking 1998) are divisible into two mappable units, a lower, white-to-buff sandstone unit and an upper red sandstone unit (Figure 7). Several local marker beds, chiefly pink micaceous, fine-grained sandstone also occur within the crater walls. Generally, these local markers can be traced no more than a few hundred metres, and none serve as a definite stratigraphic datum to tie the stratigraphy together around the circumference of the walls. A cliff-forming member of the lower sandstone unit on the north and east crater walls also fails as a stratigraphic datum, as there are rapid lithofacies changes in this member. On the east side of the crater, the cliff-forming member is almost entirely thin-bedded flaggy sandstone; however, on the north crater wall the cliff-forming member is chiefly medium-bedded and cross-bedded with only minor thin-bedded, flaggy intervals. The entire sequence of the lower buff sandstone unit appears to be fluvial in origin but no channel deposits were observed, and a marine or

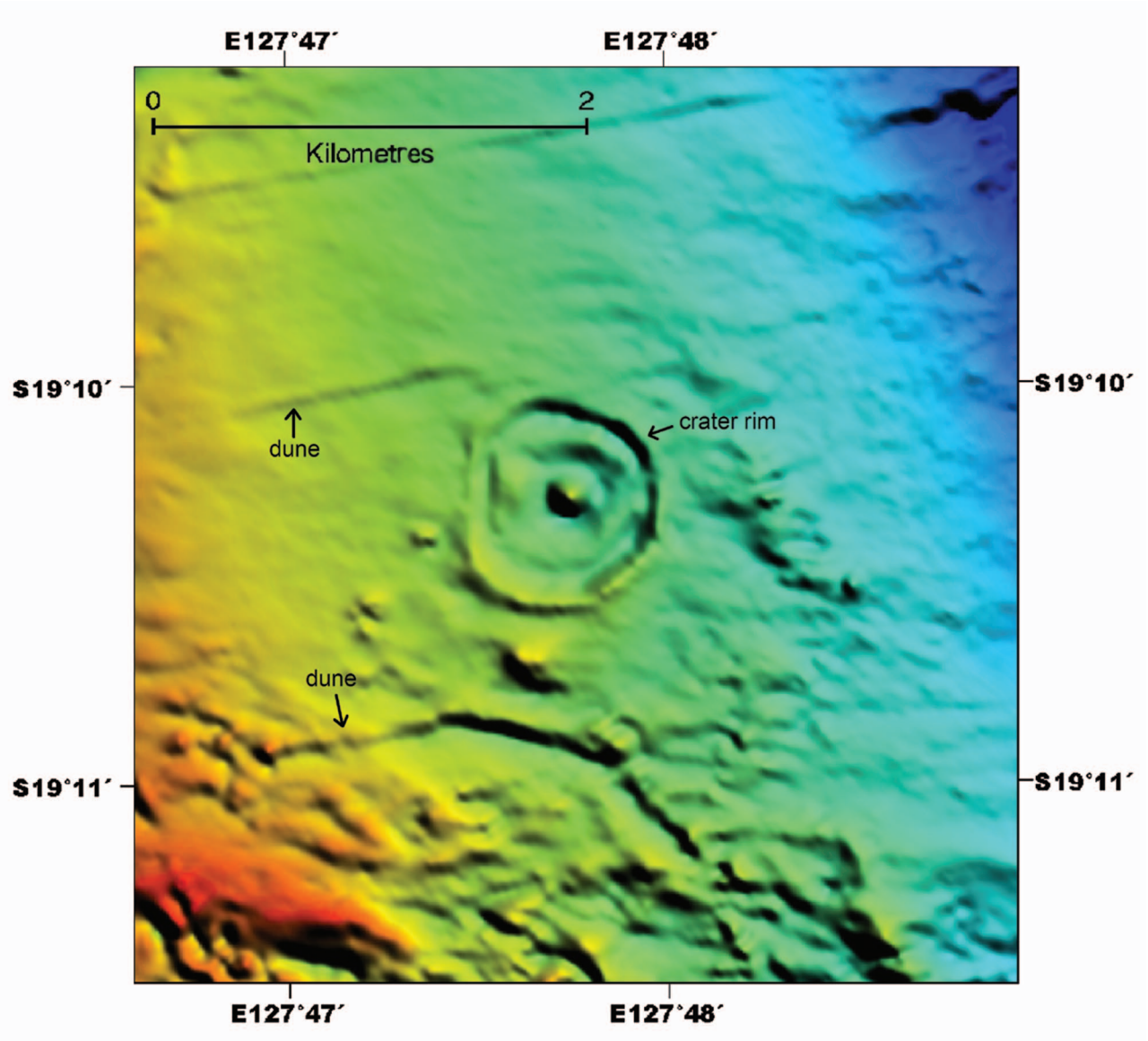

Figure 6 Aeromagnetic image of Wolfe Creek Meteorite Crater (image courtesy of R. P. Iasky and the Geological Survey of Western Australia). The line spacing is 50 m over a 4 x 4 km area, with a nominal terrain clearance of 40 m, although this varied between 30 and 60 m, especially in the crater area (R. P. Iasky pers. comm. 2004). The outer ring is an edge effect from the truncation of the highly magnetic laterite layer, the inner ring is situated approximately at the base of the crater walls under the crater fill, and the central high occurs over a concentration of gypsum-rich sink holes. The roughly east–west-trending linear features on the west side of the crater are sand dunes that 'horseshoe' around the topographic obstacle of the crater rim.

estuarine depositional environment cannot be precluded. The upper red sandstone also exhibits rapid lateral facies changes. This unit is mostly thin-bedded, fine- to very-fine-grained sandstone, and on the south rim it includes medium-bedded, fine- to medium-grained sandstone, especially at lower levels. Consequently, the contact with the underlying lower buff sandstone unit is somewhat difficult to follow, particularly as both units weather to a reddish-brown color. This problem is encountered again in attempts to map the contact between ejecta units.

Miocene laterites (Hawke 2003) are the most distinctive and easily traced map unit in the crater (Figure 7). Exposures range in thickness from about 0.3 m to 2.5 m. Sandstone in contact with the laterite is locally stained a dark purplish-red to a depth of several centimetres, but the contact is always sharp. It is sometimes difficult to distinguish true laterite from pisolitic clasts derived from the red-stained sandstone, particularly in the ejecta. The unit mapped as laterite includes blocks of both laterite and sandstone. Generally, the laterite is so thin that laterite ejecta deposits do not create a cohesive layer. On the southwestern side of the crater, shale balls (completely oxidised meteoritic iron) are commonly welded to the top of the laterite. Shale balls can also be found in ejecta units on the southwest inner crater walls (McCall 1965). Areas of concentrated shale balls

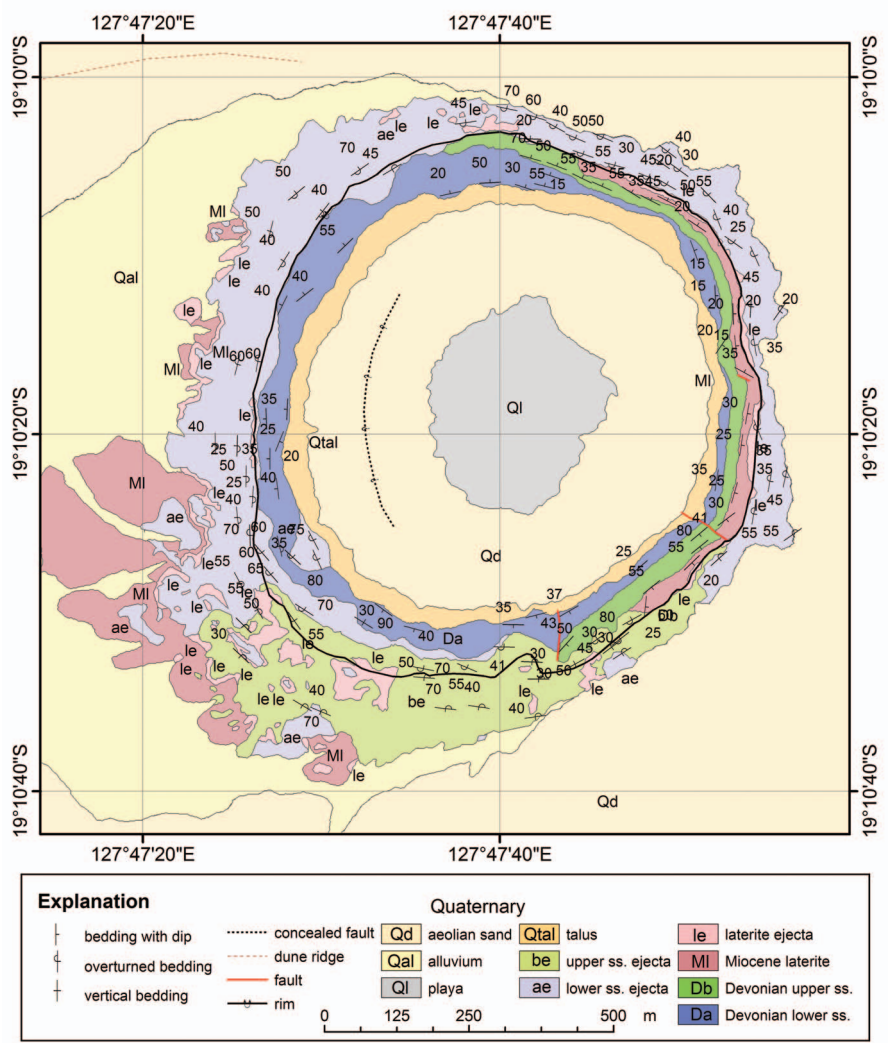

Figure 7 Geological map of the Wolfe Creek Meteorite Crater, compiled by E. M. Shoemaker in 1984. Ejecta units are divided according to their source in the wall rocks and are defined in detail in the text. The crater displays an upturned rim rolled over into an inverted stratigraphy in the ejecta. The exposure of Quaternary alluvium is the product of the topographic shelter the rim provided from aeolian sands.

seem to correlate with discrete magnetic highs on the southwest flanks of the crater rim (Figure 6).

The lower sandstone ejecta unit and the upper sandstone ejecta unit are derived from the lower buff sandstone unit and the upper red sandstone unit, respectively (Figure 7), and are exposed in an inverted stratigraphy. Local facies and lithological changes within the crater wall are also reflected in adjacent ejecta. Material ejected from the upper sandstone unit is found only on the south and east rim. Average dips of large ejecta blocks were measured where the orientation is consistent over a substantial number of observed blocks. The orientation of blocks is only locally coherent, however, and it is chaotic in much of the ejecta, particularly low on the outer flanks of the crater rim. Almost all measured dips are steeper than the basal contact of the ejecta. This is probably due in part to angular momentum of ejected blocks having sheared the ejecta layer, and also in part to viscous drag at the base of the ejecta sheet, causing the upper part to travel farther than the lower part.

Units in the crater floor include talus, aeolian sand and playa deposits. The talus appears to be Holocene and is dissected by only a few minor gullies. No older generation of talus, such as that found at Meteor Crater, was observed. The talus is overlapped by aeolian sand, which is at least partly active now. Most of this sand is exogenous to the crater, having been blown in over the eastern rim. The playa lake deposits consist of grey sand cemented with gypsum and calcite. The uppermost playa bed (exposed in a sinkhole) forms a fairly hard crust near the present playa surface. Several sinkholes in the crater floor are arranged in roughly linear chains (McCall 1965). The central magnetic high appears to be situated over the major sinkholes, which might indicate that some magnetic species are being precipitated along with the gypsum and calcite. A ring fault within the crater-fill is suggested by an arcuate pattern of vegetation. This fault could be the result of compaction, of desiccation failure, or of impact generated weaknesses deep in the crater floor.

The aeolian sand exterior to the crater includes well-formed linear dunes, but locally, it is also fluvially reworked. The crater rim constitutes a topographic obstacle to regional winds blowing from the east, and a horseshoe-shaped collar of sand wraps around the outside of the crater. The two arms of the horseshoe trail leeward from the crater flanks (McHone *et al.* 2002), analogous to patterns seen on Mars (Greeley *et al.* 1974). These dune ridges can be seen in the aeromagnetic

image (Figure 6). Miller *et al.* (2002) suggested that the magnetic signature of the dunes is due to the presence of maghemite in aeolian clays that coat sand grains. The Quaternary alluvium consists of reworked aeolian sand mixed with colluvium that is derived primarily from the ejecta units. In general this unit comprises a veneer < 1 m thick.

In oblique impact experiments, Gault and Wedekind (1978) found a focusing effect of melt and projectile ejection downrange at impactor trajectories $< 45^\circ$. We found melt glass ~ 3 km southwest of the crater, and shale balls are extremely common on the southwest side of the crater. Wolfe Creek Meteorite Crater's elliptical form, asymmetrical rollover of the rim, lop-sided ejecta pattern, and the preponderance of meteoritic material on the southwest side of the crater all indicate a moderately oblique impact ($30-45^\circ$ from the horizontal) from the northeast.

BOXHOLE METEORITE CRATER

Boxhole is an ~ 180 m-diameter meteorite crater that lies ~ 170 km northeast of Alice Springs, Northern Territory (22°36′45″S, 135°11′47″E: Figure 1). Madigan (1937) was the first to describe the crater and the medium octahedrite iron meteorites found nearby. The crater is situated along the south flank of an east–west-trending topographic ridge (Figure 3b) and is underlain by weathered, steeply dipping, Palaeoproterozoic metamorphic rocks. Pre-crater colluvium mantles the flank of the ridge and is exposed on the rim of the crater (Figure 8). Both the bedrock and the pre-crater surficial deposits have been uplifted and deformed in the walls of the crater.

We distinguished four bedrock units at the Boxhole crater (Figure 8). In descending order of structural dip (south to north) these are: (i) a quartzo-feldspathic gneiss; (ii) a muscovite–quartz–feldspar schist; (iii) a brown-weathering muscovite–quartz–feldspar schist; and (iv) vein quartz and country rock chiefly replaced by quartz. The deeply weathered quartzo-feldspathic gneiss is exposed in the southern crater walls. In weathered outcrops, gneissic banding is indistinct, and bedrock orientation is very difficult to determine, particularly on the southwest crater wall. The muscovite schist contains moderate to abundant amounts of muscovite, both in the ground mass and locally as conspicuous porphyroblasts. Schistosity is pronounced throughout this unit, facilitating the measurement of

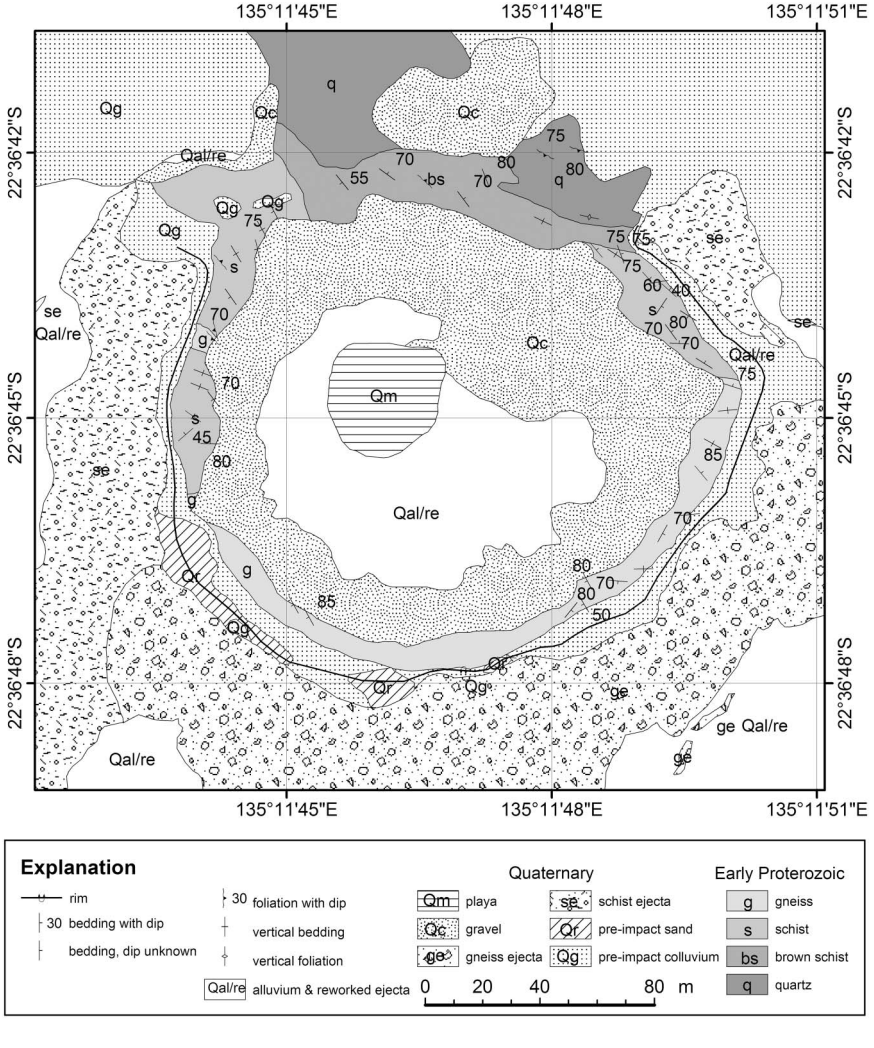

Figure 8 Geological map of the Boxhole Meteorite Crater, compiled by E. M. Shoemaker in 1987. Ejecta units are divided according to their source in the wall rocks and are defined in detail in the text. The target rock is a slope of Precambrian metamorphic rocks mantled with Quaternary colluvium.

attitudes. The contact with the gneiss runs west-southwest through the crater. Like the gneiss, the schist is deeply weathered and feldspars are largely altered to clay. Relatively fresh-appearing muscovite has survived, which distinguishes the schist both in the bedrock and the ejecta. The brown-weathering schist is a mixed unit consisting predominantly of muscovite schist, but includes some non-micaceous quartzo-feldspathic gneiss near the contact with the muscovite–quartz–feldspar schist unit (Figure 8). The brown colour may be associated with mineralisation adjacent to the zone of intense siliceous replacement represented by the main body of vein quartz. This quartz unit consists of discrete veins and replacement bodies of quartz within the other units, as well as a major throughgoing unit that underlies the ridge north of the crater and is exposed in the north crater wall (Figure 8). The mapped quartz bodies consist of complex masses of quartz veins, and quartz-replacement and residual remnants of altered host rock. Discrete quartz veins generally trend east-northeast and dip at moderate to steep angles to the south, cutting the schistosity and gneissosity of host rocks.

Two units of pre-crater surficial deposits are exposed on the southern crater rim and the northern ridge: (ii) a gravelly colluvium; and (ii) a pale reddish-brown gravelly sand. Along the rim it is difficult to distinguish these units from ejecta. Nonetheless, except for along the ridge, outside the topographic rim these units are probably ejecta as they are often associated with ejecta from the bedrock units. The gravelly colluvium consists predominantly of subangular pebbles and cobbles of brown-stained quartz derived from the vein quartz unit on the northern ridge. This colluvial deposit extends up the slope of the ridge and in places to its crest. Apparently, the colluvium also extends beneath alluvium in the floor of the valley, as shown by its presence in the crater rim. The gravelly sand unit consists of pale reddish-brown aeolian sand with subordinate subangular quartz pebbles. From its distribution on the crater rim, we infer that the gravelly sand occupies channels cut into the older colluvium.

Ejecta deposits are distinguished according to their bedrock source (Figure 8). No ejecta units corresponding to quartz or brown schist sources were identified. The ejecta blanket is thickest along the south rim crest, but is entirely absent on the north rim. Outside the rim, the ejecta blanket is often reworked and overlapped by a veneer of post-impact alluvium. Extensive ejecta can be traced to more than 300 m south of the crater (Roddy *et al.* 1988) (Figure 3b), but in order to show details of the crater walls, we have not illustrated the complete extent of ejecta on the geological map (Figure 8). The asymmetries in both the crater rim and ejecta distribution could either be the product of an oblique impact from the north or the pre-existing topography and structure of the quartzite ridge along the northern crater rim.

Post-impact units include a Quaternary colluvium, alluvium and playa deposits. This younger colluvium is derived both from the wind-blown sand and from older colluvium on which it rests. The post-impact alluvium is composed largely of reworked ejecta, particularly south of the crater where it becomes difficult to distinguish undisturbed ejecta deposits from reworked ejecta.

Milton (1972) suggested that the Boxhole Meteorite Crater was formed in a joint fall with the Henbury Meteorite Craters located ~250 km to the southwest. The meteorites at both sites are of the iron group IIIAB (Bevan 1996). Moreover, Kohman and Gohl (1963) presented indistinguishable terrestrial radiogenic carbon ages for the meteorites at Boxhole crater of 5400 ± 1500 a and those at the Henbury craters of 4200 ± 1900 a. However, these dates were acquired before accelerator mass spectrometry techniques were developed (Gove 1992). More recently, Shoemaker *et al.* (1990) obtained a ^{10}Be-^{26}Al exposure age of *ca* 30 ka from a resistant quartz vein in the crater wall and from a quartz block in the ejecta. Furthermore, as we discussed above, unless all the asymmetries in the crater form and ejecta at Boxhole are due to pre-existing structure, it appears that the impactor struck obliquely from the north, whereas the Henbury crater field was formed by an oblique impact from the southwest (Milton 1972). We prefer the older date of the Boxhole crater not only because of the improved analytical techniques, but also because the ejecta blanket at the Henbury craters is markedly less degraded than that at Boxhole (Shoemaker *et al.* 1988). Extremely low weathering rates are needed to reconcile this older date and the excellent preservation of the crater walls at Boxhole. Cosmogenic radionuclide analyses on quartzites in the nearby Davenport Ranges yielded an erosion rate of 0.34 ± 0.03 m per million years (Belton *et al.* 2004).

VEEVERS METEORITE CRATER

Veevers Meteorite Crater is located in the Great Sandy Desert of Western Australia (22°58′06″S, 125°22′07″E: Figure 1). The ~70-m crater was discovered in 1975 by A. N. Yeates (Yeates *et al.* 1976). In all respects, Veevers Meteorite Crater may be one of the best-preserved terrestrial impact craters known. A cosmogenic nuclide exposure age of < 20 ka from crater wall laterites was obtained (E. M. Shoemaker pers. comm. 1995 *in* Glikson 1996); however, Shoemaker and Shoemaker (1988) suggested a younger age of < 4 ka on the basis of the pristine form of the ejecta blanket.

Cenozoic laterite is exposed in the walls of the Veevers crater (Figure 9). The laterite is composed of pisolites and nodules ranging from about 2 mm to 6 cm in diameter. The laterite has a crude platy structure, which prior to deformation was subhorizontal. This platy structure is defined chiefly by fractures that opened during weathering, and where well developed it is possible to measure attitudes of the fractures with a precision of 5–10°. Regionally, laterite is developed on Cretaceous bedrock, but the base of the laterite is not exposed within the crater. The total thickness of exposed laterite is ~10 m. An upper, dark mottled zone was differentiated from the rest of the laterite. This zone represents the ground surface at the time of the impact, and it can be traced almost continuously around the crater, varying in thickness from ~30 cm to ~1 m.

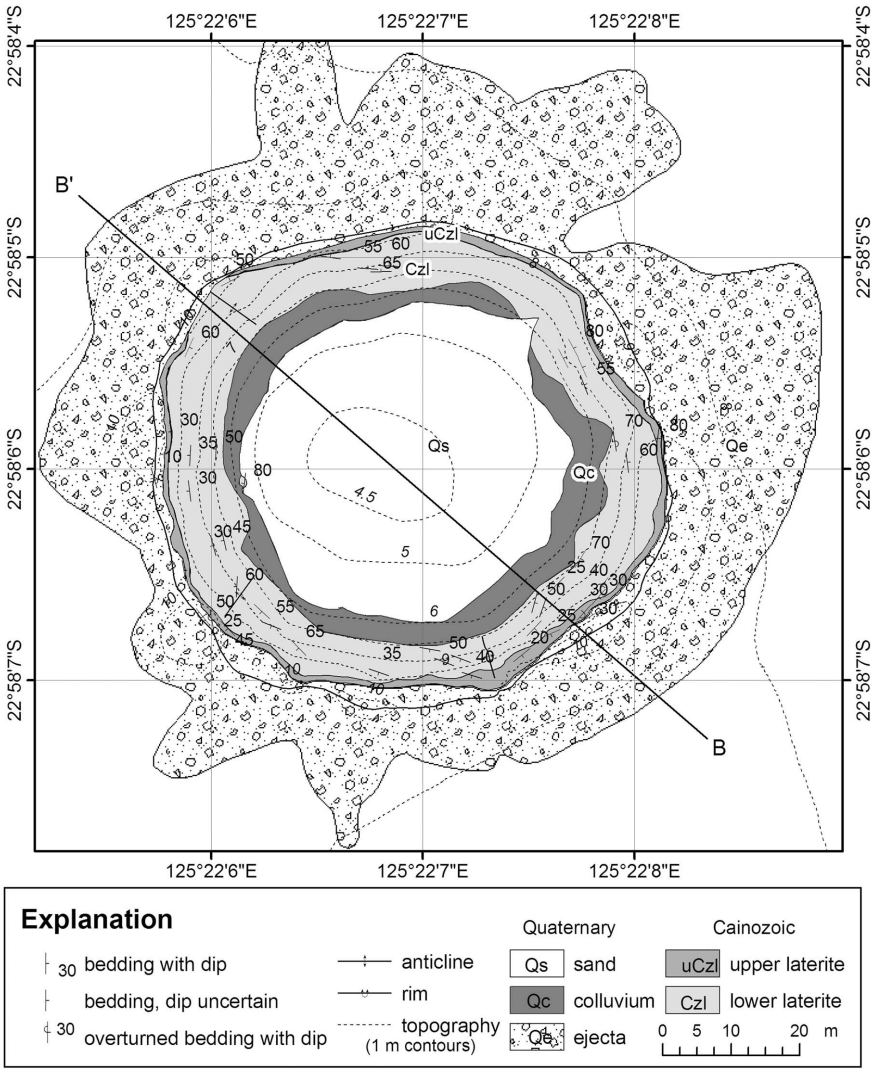

Figure 9 Geological map of the Veevers Meteorite Crater, compiled by E. M. Shoemaker in 1986. The Veevers crater is exceptionally well preserved, and the lobes apparent in the ejecta unit (Qe) are not erosional remnants, but rather preserved rays with blocks strewn radially. Topographic contours are at a 1 m interval relative to an arbitrary base, with an additional 4.5 m contour in the centre of the crater. See Figure 10 for cross-section B–B'.

The Veevers ejecta consist of blocks and nodules of laterite. Commonly, a veneer of loose nodules coats the weathered surface of the ejecta. The contact between the ejecta and upturned laterite is generally close to the rim crest, but lies somewhat below the crest on the west wall. Blocks of laterite (< 0.65 m across) are exposed on the south rim where the ejecta are thicker and appear to be better preserved. The ejecta form 12 distinct ray-like lobes that commonly radiate from discrete high points on the crater rim. Preservation of subtle morphology in the ejecta blanket confirms an unusually young age for the crater. One significant morphological change has taken place, however. The crater floor has been filled by aeolian sands blown in from the southwest. This crater fill sand climbs about half-way up the northeast crater wall toward the rim crest. The superimposed exterior sand sheet consists of colluvially reworked aeolian sand with grains and nodules derived from underlying laterite and ejecta. Quaternary colluvium occurs on the lower crater wall and consists mostly of loose nodules and scattered blocks of laterite that have tumbled in from higher on the crater walls.

Laterite slabs are upturned all around the crater wall, although uplift of the rim has not been uniform in all directions. Three distinctive outward-plunging anticlines can be recognised, the largest of which occurs on the northwest side (Figure 9). The rim crest extends distinctly outward over the northwest anticline and forms a rounded corner in the outline of the crater. On the opposite crest, laterite near the hinge line dips outward rather gently (25—30°). Elsewhere, ejected laterite is overturned abruptly. Dips do not progressively increase up the crater walls, but are generally steepest low on the exposed walls and become shallower close to the hinge line and ejecta unit (Figures 9, 10). This relationship indicates that observed dips are due to frictional drag along the wall of a transient cavity, as observed at the Jangle U high-explosive test crater (Shoemaker 1963).

In 1986, we undertook a detailed magnetic survey across Veevers Meteorite Crater to determine if a large meteoritic mass was preserved in the crater. A steep negative vertical gradient within the main anomaly in the crater (at depths beginning at about ground level) showed unequivocally that magnetic anomalies origi-

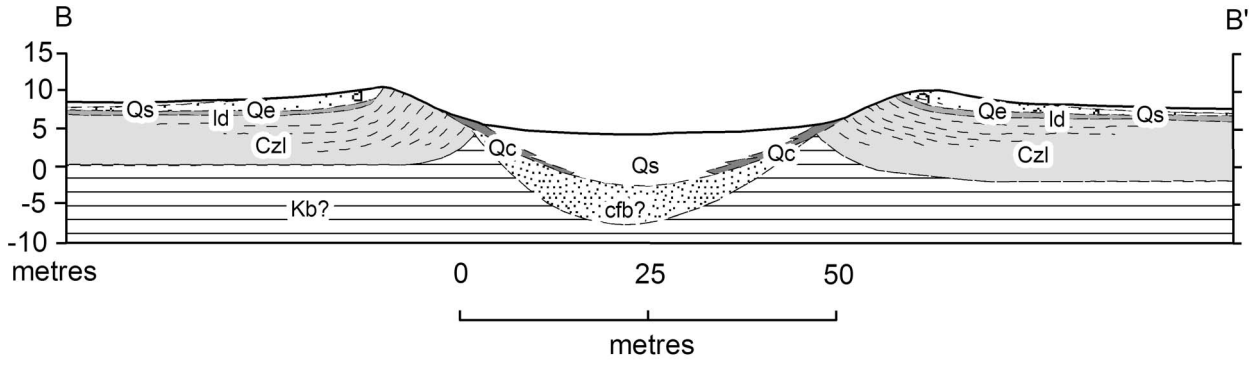

Figure 10 Northwest–southeast geological cross-section of the Veevers Meteorite Crater (see Figure 9 for location). Note the lack of a complete rollover in the crater walls and the slight offset to the northwest of the crater floor. The positions of the crater-fill breccia (cfb?) and Cretaceous bedrock (Kb?) are assumed. The rim height, and the position of contacts and thicknesses of units at depth were estimated by projecting from attitudes of bedding planes and contact surfaces exposed in the crater walls. Elevations are relative to an arbitrary base.

nate from the colluvium. If a meteoritic signal is present, it is submerged in the colluvium anomaly. It is clear that there are no large (i.e. several tonnes) meteorites present at depth. As the mass of a projectile required to form this crater is probably in the range 100–1000 t (depending on assumed velocity), the meteorite evidently was shattered into small fragments that were dispersed into a breccia lining the crater floor (Bevan *et al*. 1995). The Veevers crater is exceptionally well preserved and has been modified only very slightly by erosion. Hence, it seems unlikely that much meteoritic material has been lost by downwasting and lateral transport. The scarcity of meteorites, and absence of iron-rich shale balls, impactites, and melt spherules indicates that the impactor velocity was minimal, perhaps slowed below escape velocity by atmospheric drag. In which case, the total mass of meteoritic material may be closer to the 1000 t estimate (but dispersed in the breccia lens).

DALGARANGA CRATER

Dalgaranga crater (27°40′00″S, 117°17′30″E: Figure 1) is ~24 m in diameter and ~3 m deep (Figure 11). In 1923, G. E. P. Wellard discovered stony-iron meteorites at Dalgaranga (Bevan 1996). Later, H. H. Nininger collected more than 9 kg of mesosiderite meteorites from shallow trenches in the crater (Nininger & Huss 1960). In 1986, we cleaned and deepened Nininger's original pit located near the eastern edge of the crater floor. In order to accurately determine crater composition and dimensions, and to confirm that basement had been reached, excavation continued about 0.5 m into the underlying breccia lens (Figure 12).

The crater walls are formed primarily in badly decomposed Archaean granite. On the southwest side, where the granite is freshest, it is medium grained and quartz-rich, verging on alaskite, with quartz content at ~50%. Elsewhere, the granite's feldspars have been altered to clay minerals, and on the east and north sides of the crater, the granite is partially lateritised. A nascent pisolitic structure, extensively developed in the more deeply weathered granite on the northwest crater walls, prompted Nininger to call it laterite (Nininger & Hess 1960). Some true laterite is present just below the surficial unit and in breccia blocks, but most blocks exposed on the north and east walls are still recognisable as granite. In many places, the severely weathered granite bedrock has decomposed into coarse-grained quartz sand with a clay-rich matrix. Granite near the surface is sheeted with spacing ranging from a few centimetres to ~30 cm. Sheeting makes it possible to determine target rock attitudes within the crater walls.

The breccia unit is extensively exposed around the southwest half of the crater wall and on the east wall in Nininger's excavation (Figure 11). The breccia is composed chiefly of weathered granite, but it also includes fragments of the surficial unit and laterite. Breccia clasts range in size from < 1 cm to 0.5 m or more. On the southwest side of the crater, the breccia is composed exclusively of granite. Large displacements and mixing of breccia blocks is more evident in the eastern exposures, particularly in the pit. Near the crater centre, a block of Quaternary surface material is embedded within the breccia, indicating a downward displacement of breccia materials during the impact event.

The blocky talus is a surficial unit that mantles the lower part of the northern crater wall. The talus includes very large blocks including one more than 2 m across that is situated at the base of the east wall. The attitudes of clasts are somewhat chaotic, although platy clasts tend to lie parallel to the wall. In contrast to the breccia, which is compact, the talus unit comprises relatively loose pieces that appear to have slid back down along the crater wall. The contact between the talus and breccia units is well exposed in Nininger's pit. Above the talus, 9.1 m of colluvium is exposed in the pit. The colluvium consists predominantly of sand-sized quartzite grains and weathered granitic detritus, and is nearly massive, but shows a weak planar structure due to the crude alignment of tabular blocks of weathered granite, some more than 0.5 m across.

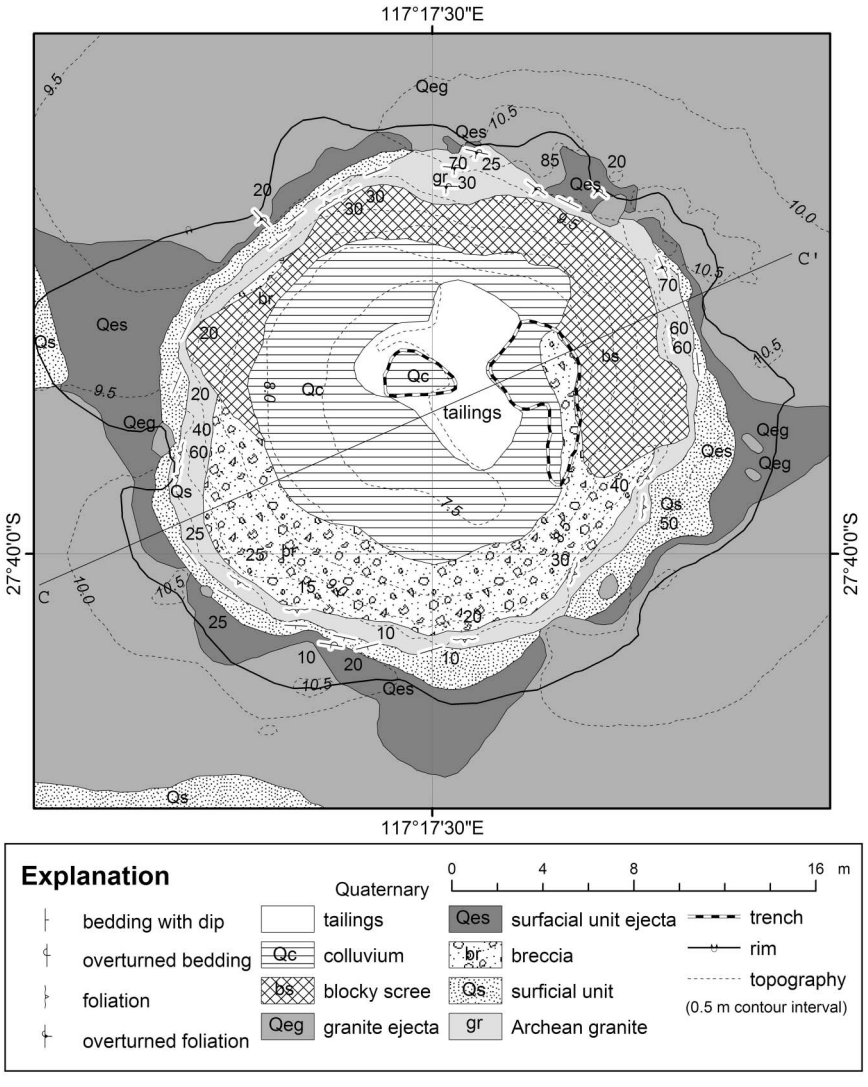

Figure 11 Geological map of the Dalgaranga crater, compiled by E. M. Shoemaker in 1986. The ejecta at Dalgaranga display a marked symmetry along a north-northeast–south-southwest axis, with very little ejecta directly uprange, two uprange rays at a 60° angle to the impact azimuth, and two 'forbidden zones' at 90° from the direction of impact. Topographic contours are at 0.5 m interval relative to an arbitrary base. See Figure 12 for cross-section C–C'.

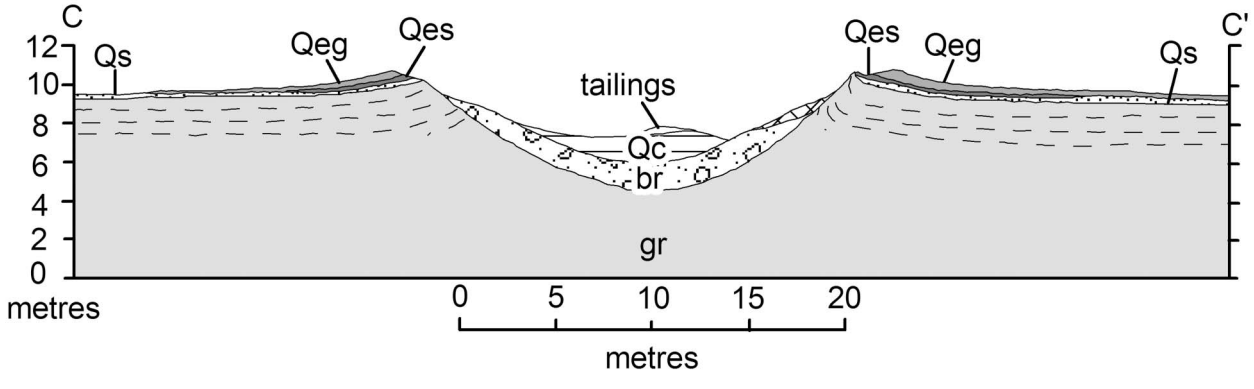

Figure 12 Geological cross-section of the Dalgaranga crater (see Figure 11 for location). The rim height, and the position of contacts and thicknesses of units at depth were estimated by projecting from attitudes of bedding planes and contact surfaces exposed in the crater walls. Elevations are relative to an arbitrary base.

The Quaternary surficial unit is a prominent marker that makes it possible to define the rim structure and hinge line. In general, this unit rests in sharp contact on the granite, and therefore is not merely a weathering horizon. The surficial unit is 20–50 cm thick, and is crudely stratified, which makes it possible to accurately measure attitudes. The surficial unit is composed of ~50% coarse-grained quartz set in a porous matrix of

fine- to medium-grained quartzite, bound by siliceous cement.

The ejecta deposit of weathered granite blocks is largely chaotic, although close to the rim many tabular clasts derived from sheeted granite are nearly horizontal. These almost certainly are overturned, and are demonstrably so where a portion of the surficial unit is still attached. A few clasts more than a metre across are present, but most are ~0.5 m or smaller. Most of the large blocks are on the northeast rim, a few of which have been thrown more than 20 m from the rim. The ejecta unit composed of surficial-unit blocks underlies the granite ejecta and rests directly on the Quaternary surficial deposit. At the hinge line, the surficial ejecta blocks are abruptly overturned and are gently dipping along most of the crater rim. On the north side the Quaternary surficial ejecta is tilted up more steeply, and is locally overturned and concealed beneath granite ejecta. The more complete rollover of these rim and ejecta units on the north side of the crater is consistent with the inferred direction of impact from the south-southeast. The extreme bilateral symmetry of the ejecta units, with a large 'forbidden' zone uprange and with two pronounced uprange rays (at a ~60° angle from the incoming impactor azimuth: Figure 11) is similar to laboratory experiments for an angle of incidence between 10° and 15° above the horizontal (Gault & Wedekind 1978). The preservation of subtle morphology in the ejecta led Shoemaker and Shoemaker (1988) to estimate that the Dalgaranga crater was formed < 3000 years ago.

DISCUSSION AND CONCLUSIONS

Although we are able to measure crater and ejecta dimensions and composition of target rocks (Table 1), it is very difficult to calculate the size of the meteorite that made the craters, because crater size depends upon projectile size, type, speed, and the angle at which it struck. Our observations give us some handle on the angle of incidence, but scaling relations still leave us with the two unknown variables of size and speed of the impactor. Moreover, the choice of which scaling law to use becomes controversial over the size range of the craters presented herein, where there is a transition between strength and gravity-dominated craters (Melosh 1988). Consequently we shy away from scaling the size of the impactors and stick with the observations (Table 1).

In the present study we distinguish between Barringer- and Odessa-types of small craters based primarily on the slope and structure of the wall rocks, the projected geometry of the floor and the form of the rim rocks. Particularly, like the Barringer crater, Liverpool crater and Wolfe Creek Meteorite Crater have steep walls (~45°) and thick breccia lenses. Wolfe Creek Meteorite Crater also has a flat floor and a rim composed of overturned bedrock. These features imply substantial late stage gravity modification. While neither the Boxhole, Veevers, nor Dalgaranga craters display obvious rim anticlines like observed at Odessa, at least at Veevers Meteorite Crater, dips clearly decrease up the crater wall. Moreover, all three craters have shallow walls (~30°) which project to bowl-shaped floors, and the wall rock of the rims appear to be truncated with the crest commonly composed of ejecta.

Structural differences between Odessa and Barringer crater types are due in part to depth of penetration of the meteorite. Two nuclear explosion craters in alluvium at the Nevada Test Site, Jangle U and Teapot ESS, illustrate the importance of penetration depth. Both craters were formed by explosions of the same yield (1.2 kt) but detonated at different depths. In the Jangle U experiment, a burst at ~5.2 m below the ground surface produced a crater of the Odessa type, whereas in the Teapot ESS experiment, detonation at a depth of ~20.4 m produced a crater of the Barringer type (Shoemaker 1963). An explosion at a shallow depth forms a crater more through radial expansion of the cavity behind the shock and less by ejection of material, with the greatest expansion occurring at the surface, manifesting itself in concentric anticlinal buckling (Shoemaker 1963). As the meteorites and target rocks at the Barringer and Odessa craters are similar, the indicated difference in the scaled depth of penetration can be accounted for by difference in impact velocity, with the smaller Odessa meteorite mass having encountered greater drag passing through the atmosphere (Shoemaker 1963). However, penetration depth is only one of many operative variables in impact cratering. In particular, crater form is also largely dependent on impact angle and target strength.

Effectively, all planetary impacts are oblique to some degree, with a modal angle of incidence of 45°, whereas vertical and grazing impacts are rare (Gilbert 1893; Shoemaker 1962). An approximate direction of impact can be ascertained at all of the small Australian craters that we studied, due to marked geometric asymmetries at each. The most obvious signature of an oblique impactor trajectory is asymmetric ejecta distribution (Gault & Wedekind 1978; Schultz & Anderson 1996). Experimentalists have found that a missing pie-slice sector of uprange ejecta accompanies impact angles less than ~30° from the horizontal, and that the radial angle of missing ejecta increases as impact angle decreases (Schultz & Anderson 1996). Based on Gault and Wedekind's (1978) experimental results, we have extrapolated an approximate angle of impact from the ejecta patterns (Table 1). At all of the craters that we studied, the estimated direction of impact is supported by asymmetries in the structural form of the crater walls.

Target strength is an important variable in impact cratering (Melosh 1989), and the craters we studied are developed in a variety of targets, ranging from brittle sandstones at Wolfe Creek Meteorite Crater to loosely consolidated laterites at Veevers Meteorite Crater to deeply weathered Archaean granites at Dalgaranga crater. Boxhole Meteorite Crater's structure is complicated by its position along a slope of resistant, foliated quartzites, which are mantled by unconsolidated colluvium. As the projectile width was probably roughly equivalent to surficial colluvium depth at Boxhole, cover sediments likely had little effect on the crater form. However, the slope and structure of the underlying basement rocks may have contributed to the asymmetrical ejecta pattern.

Among the impact craters identified on Earth, no two are identical. The rich variety of features displayed by the small Australian craters we studied arises from the numerous variables at work in the cratering process. Such variability indicates that even subtle differences in impact conditions can have profound structural effects on the resultant crater. These differences are apparent not only between different impact localities, but also within single crater fields, such as Henbury, where a spectrum of crater forms is present (Milton 1978). Such a variety of crater forms belies the simplified impact cratering models that are analogous to point-source explosions at different burial depths. Australia's extensive collection of well-preserved small craters facilitates further comparative study. While many questions remain, the data and interpretations presented herein constitute a framework to constrain further theoretical studies of impact-cratering processes.

ACKNOWLEDGEMENTS

We would like to thank the Thomas J. Watson Fellowship Foundation and the Barringer Crater Company for support to FAM. We are also grateful to Alex Bevan, Michael Dence, John McHone, Jay Melosh and Wyllie Poag for helpful comments, Robert Iasky for aeromagnetic images, Trent Hare for GIS assistance, and the USGS Astrogeology Program for the use of their facilities. CSS has so many people to thank for helping her and Gene during their 12 years of fieldwork in Australia, that it is impossible to list them all here.

REFERENCES

Bevan A. W. R. 1996. Australian crater-forming meteorites. *In:* Glikson A. Y. ed. *Australian Impact Structures*, pp. 421–429. AGSO Journal of Australian Geology & Geophysics **16**.

Bevan A. W. R., Shoemaker E. M. & Shoemaker C. S. 1995. Metallography and thermo-mechanical treatment of the Veevers (IIAB) crater-forming meteorite. *Records of the Western Australian Museum* **17**, 51–59.

Belton D. X., Brown R. W., Kohn B. P., Fink D. & Farley K. A. 2004. Quantitative resolution of the debate over antiquity of the central Australian landscape: implications for the tectonic and geomorphic stability of cratonic interiors. *Earth and Planetary Sciences* **219**, 21–34.

Carson L. J., Haines P. W., Brakel A., Pietsch B. A. & Ferenczi P. A. 1999. *Milingimbi, Northern Territory, 1:250 000 Geological Map Series, Sheet SD53-2.* Northern Territory Geological Survey, Darwin.

Evans G. E. & Mear C. E. 2000. The Odessa meteor craters and their geological implications. *Occasional Papers of the Strecker Museum* **5**.

Fudali R. F. 1979. Gravity investigation of Wolf Creek Crater, Western Australia. *Journal of Geology* **87**, 55–67.

Gault D. E. & Wedekind J. A. 1978. Experimental studies of oblique impact. *Proceedings of the 9th Lunar and Planetary Science Conference*, 3843–3875.

Gilbert G. K. 1893. The moon's face, a study of the origin of its features. *Bulletin of Philosophical Society of Washington DC* **12**, 241–292.

Glikson A. Y. 1996. A compendium of Australian impact structures, possible impact structures, and ejecta occurrences. *In:* Glikson A. Y. ed. *Australian Impact Structures*, pp. 373–375. AGSO Journal of Australian Geology & Geophysics **16**.

Gove H. E. 1992. The history of AMS, its advantages over decay counting; applications and prospects. *In:* Taylor R. E., Long A. & Kra R. S. eds. *Radiocarbon after Four Decades; an Interdisciplinary Perspective*, pp. 214–229. Springer-Verlag, New York.

Guppy D. J., Brett R. & Milton D. J. 1971. Liverpool and Strangways craters, Northern Territory; two structures of probable impact origin. *Journal of Geophysical Research* **76**, 5387–5393.

Greeley R., Iversen J. D., Pollack J. B., Udovich N. & White B. 1974. Wind tunnel studies of Martian aeolian processes. *Proceedings of the Royal Society of London* **341**, 331–360.

Hawke P. J. 2003. Geophysical Investigation of the Wolfe Creek Meteorite Crater. *Geological Survey of Western Australia Record* **10**, 1–9.

Kohman T. P. & Gohl P. S. 1963. Terrestrial ages of meteorites from cosmogenic C14. *In: Radioactive Dating*, pp. 395–311. International Atomic Energy Agency, Vienna.

Madigan C. T. 1937. The Boxhole Crater and the Huckitta Meteorite (central Australia). *Transactions and Proceedings of the Royal Society of South Australia*, **6**, 187–190.

McCall G. J. H. 1965. Possible meteorite craters—Wolfe Creek, Australia and analogs. *New York Academy of Sciences Annual* **123**, 970–998.

McHone J. F., Greeley R., Williams K. K., Blumberg D. G. & Kuzmin R. O. 2002. Space shuttle observations of terrestrial impact structures using SIR-C and X-SAR radars. *Meteoritics and Planetary Science* **37**, 407–420.

Melosh H. J. 1989. *Impact Cratering: a Geologic Process*. Oxford University Press, New York..

Miller E., Miller G., Johnson B., Fogel M., Magee J., Spooner N., Creasy J. & Bryant M. 2002. Examination of surface features and mineralogy of quartz grains from Wolfe Creek Crater, Western Australia to determine provenance as an indicator of paleoclimate. *Geological Society of America, Northeastern Section, 37th Annual Meeting*, abstract 31820.

Milton D. J. 1972. Structural geology of the Henbury meteorite craters, Northern Territory, Australia. *US Geological Survey Professional Paper* **599-C**, c1–c17.

Myers J. S. & Hocking R. M. 1998. *Geological map of Western Australia 1:2 500 000* (13th edition). Geological Survey of Western Australia, Perth.

Nininger H. H. & Huss G. I. 1960. The unique meteorite crater at Dalgaranga, Western Australia. *Mineralogical Magazine* **32**, 619–639.

Reeves F. & Chalmers R. O. 1949. The Wolf Creek crater. *Australian Journal of Science* **11**, 145–156.

Rix P. 1965. *Milingimbi, Northern Territory, 1:250 000 Geological Series, Sheet SD/532*. Bureau of Mineral Resources, Canberra.

Roddy D. J., Shoemaker E. M., Shoemaker C. S. & Roddy J. K. 1988. Aerial photography and geologic studies of impact structures in Australia. *Lunar and Planetary Science Conference XIX*, abstract 990.

Schultz P. H. & Anderson R. R. 1996. Asymmetry of the Manson impact structure: evidence for the impact angle and direction. *In:* Koeberl C. & Anderson R. R. eds. *The Manson Impact Structure, Iowa: Anatomy of an Impact Crater*, pp. 397–417. Geological Society of America Special Paper **302**.

Shoemaker E. M. 1962. Interpretation of lunar craters. *In:* Kopal Z. ed. *Physics and Astronomy of the Moon*, pp. 283–359. Academic Press, New York.

Shoemaker E. M. 1963. Impact mechanics at Meteor Crater, Arizona. *In:* Middlehurst B. M. & Kuiper G. P. eds. *The Moon, Meteorites and Comets*, pp. 301–336. University of Chicago Press, Chicago.

Shoemaker E. M. & Eggleton R. E. 1961. Terrestrial features of impact origin. *In:* Nordyke M. D. ed. *Proceedings of the Geophysical laboratory/Lawrence Radiation Laboratory Cratering Symposium*, pp. A-1–27. Lawrence Radiation Laboratory, Livermore.

Shoemaker E. M., Roddy D. J., Shoemaker C. S. & Roddy J. K. 1988. The Boxhole Meteorite Crater, Northern Territory, Australia. *Lunar and Planetary Science Conference XIX*, abstract 1081–1082.

Shoemaker E. M. & Shoemaker C. S. 1988. Impact structures of Australia. *Lunar and Planetary Science Conference XIX*, abstract 1079–1080.

Shoemaker E. M. & Shoemaker C. S. 1997. Notes on the geology of Liverpool Crater, Northern Territory, Australia. *Lunar and Planetary Science Conference XXVIII*, abstract 311–312.

SHOEMAKER E. M., SHOEMAKER C. S., NISHIIZUMI K., KOHL C. P., ARNOLD J. R., KLEIN J., FINK D., MIDDLETON R., KUBIK P. W. & SHARMA P. 1990. Ages of Australian meteorite craters; a preliminary report. *In*: *53rd Annual Meeting of the Meteoritical Society, Abstracts*, p. 409. Meteoritics **25**.

YEATES A. N., CROWE R. W. A. & TOWNER R. R. 1976. The Veevers Crater: a possible meteoritic feature. *BMR Journal of Australian Geology & Geophysics* **1**, 77–78.

Received 29 May 2004; accepted 17 March 2005